Heliyon 6 (2020) e05116

Contents lists available at ScienceDirect

Heliyon

journal homepage: www.cell.com/heliyon

Research article

Characterization of local SARS-CoV-2 isolatesand pathogenicity in IFNAR$^{-/-}$ mice

Alireza Hanifehnezhad [a], Ebru Şahin Kehribar [b], Sıdıka Öztop [c], Ali Sheraz [b], Serkan Kasırga [b], Koray Ergünay [d], Sevgen Önder [e], Erkan Yılmaz [f], Doruk Engin [f], T. Çiğdem Oğuzoğlu [a], Urartu Özgür Şafak Şeker [b], Engin Yılmaz [g], Aykut Özkul [a,f,*]

[a] Ankara University, Faculty of Veterinary Medicine, Department of Virology, Ankara 06110 Turkey
[b] Bilkent University, UNAM–Institute of Materials Science and Nanotechnology, National Nanotechnology Research Center, Ankara 06800 Turkey
[c] Department of Immunology, Başkent University, Adana Dr Turgut Noyan Application and Research Center, Adana 01240 Turkey
[d] Hacettepe University, Faculty of Medicine, Department of Medical Microbiology, Virology Unit, Ankara 06100 Turkey
[e] Hacettepe University, Faculty of Medicine, Department of Pathology, Ankara 06100 Turkey
[f] Ankara University, Biotechnology Institute, Ankara 06135 Turkey
[g] Hacettepe University, Faculty of Medicine, Department of Medical Biology (ret.), Ankara 06100 Turkey

ARTICLE INFO

Keywords:
Bioinformatics
Microbiology
Virology
Viral disease
Viral genetics
Epidemiology
Respiratory system
SARS-CoV-2
Isolate
Genome
IFNAR$^{-/-}$ mice

ABSTRACT

The severe acute respiratory syndrome coronavirus 2 (SARS-CoV-2) recently a global pandemic with unprecedented public health, economic and social impact. The development of effective mitigation strategies, therapeutics and vaccines relies on detailed genomic and biological characterization of the regional viruses. This study was carried out to isolate SARS-CoV-2 viruses circulating in Anatolia, and to investigate virus propagation in frequently-used cells and experimental animals. We obtained two SARS-CoV-2 viruses from nasopharngeal swabs of confirmed cases in Vero E6 cells, visualized the virions using atomic force and scanning electron microscopy and determined size distribution of the particles. Viral cytopathic effects on Vero E6 cells were initially observed at 72 h post-inoculation and reached 90% of the cells on the 5th day. The isolates displayed with similar infectivity titers, time course and infectious progeny yields. Genome sequencing revealed the viruses to be well-conserved, with less than 1% diversity compared to the prototype virus. The analysis of the viral genomes, along with the available 62 complete genomes from Anatolia, showed limited diversity (up to 0.2% on deduced amino acids) and no evidence of recombination. The most prominent sequence variation was observed on the spike protein, resulting in the substitution D614G, with a prevalence of 56.2%. The isolates produced non-fatal infection in the transgenic type I interferon knockout (IFNAR$^{-/-}$) mice, with varying neutralizing antibody titers. Hyperemia, regional consolidation and subpleural air accumulation was observed on necropsy, with similar histopathological and immunohistochemistry findings in the lungs, heart, stomach, intestines, liver, spleen and kidneys. Peak viral loads were detected in the lungs, with virus RNA present in the kidneys, jejunum, liver, spleen and heart. In conclusion, we characterized two local isolates, investigated in vitro growth dynamics in Vero E6 cells and identified IFNAR−/− mice as a potential animal model for SARS-CoV-2 experiments.

1. Introduction

The year 2020 has witnessed the emergence and spread of a novel virus pandemic, called as the Corona Virus Disease 2019 (COVID-19). The infection started as an epidemic in late 2019 in China, and has turned out to affect over 4.7 million people in 216 countries as of May 20th, 2020 (World Health Organization, 2020). The causative agent has been officially named as the severe acute respiratory syndrome coronavirus 2 (SARS-CoV-2) (Coronaviridae Study Group of the International Committee on Taxonomy of Viruses, 2020). It is classified in the *Betacoronavirus* genus among other genera in family *Coronaviridae* (order Nidovirales). Similar to other coronaviruses, SARS-CoV-2 virions are enveloped, and possess a large, single-strand, positive-sense RNA genome. The ORFs in the viral genome encode for 16 non-structural proteins as well as the spike (S), membrane (M), envelope (E) and nucleocapsid (N) proteins of the mature virion (Study group, 2020). In

* Corresponding author.
E-mail address: ozkul@ankara.edu.tr (A. Özkul).

https://doi.org/10.1016/j.heliyon.2020.e05116
Received 27 July 2020; Received in revised form 20 August 2020; Accepted 25 September 2020

nature, coronaviruses are zoonotic and widely-distributed agents, affecting human, livestock, birds, bats, mice and other animals, infecting cells of the respiratory, gastrointestinal and central nervous systems of the affected species (Chen et al., 2020). In humans, six coronaviruses have so far been documented to cause symptomatic disease. Among these, F229E, HKU1, NL63 and OC43 coronaviruses are involved in flu-like disease in immune-competent individuals (Su et al., 2016). However, the acute respiratory syndrome coronavirus (SARS-CoV) and the Middle East respiratory syndrome coronavirus (MERS-CoV) are associated with severe diseases of the lower respiratory tract (Tang et al., 2020). SARS-CoV-2 also affects the lower respiratory track, causing potentially-fatal pneumoniae in individuals with underlying conditions, but produces a generally-milder disease. Current information indicates that SARS-CoV-2 is of zoonotic origin, similar to SARS-CoV and MERS-CoV (Cui et al., 2019; Andersen et al., 2020). Currently, COVID-19 lacks an evidence-based specific treatment while antiviral therapy combined with various measures for supportive care remains as the main strategy worldwide (Tang et al., 2020).

Five months after the emergence, it became apparent that health COVID-19 is a global public health threat. The economic and social impact of this pandemic is unprecedented and will likely to continue in years to come. Huge global effort is currently directed at investigating and developing efficient therapeutics and vaccines for COVID-19 (World Health Organization, 2020). Key information for these goals will be provided by detailed genomic and biological characterization of the regional viruses. They will further facilitate a deeper understanding of the ongoing virus evolution for better clinical intervention and mitigation strategies. This study was carried out to isolate SARS-CoV-2 viruses circulating in Anatolia, to investigate dynamics of virus propagation in frequently-used cells and experimental animals.

2. Materials and methods

2.1. Ethical statement

Samples used for virus isolation were collected at the Infectious Disease Clinics, Ankara City Hospital with the official permission from Ministry of Health, Ankara City Hospital, Ethical Committee for Human Experiments (20–654, 21.05.2020). The samples transferred to the laboratory in ice and biologically-sealed conditions. Infectivity studies in IFNAR−/− mice were performed with official permission from the Ankara University Ethical Committee for Animal Experiments (06 May 2020, 20120-8-66) in the high containment animal facility (Animal Biosafety Level 3 plus - ABSL3+) of the department. The animal samplings were conducted according to the national regulations on the operation and procedure of animal experiments' ethics committees (regulation no. 26220, 9 September 2006). The mice were humanely euthanized by CO_2 exposure and cervical dislocation.

2.2. Samples, virus isolation and cultivation

Nasopharyngeal swabs from individuals with real-time reverse transcription polymerase chain reaction (RT-PCR)-confirmed COVID19 were transported in Dulbecco's modified Eagle's medium (DMEM; Lonza, USA), supplemented with 10% fetal bovine serum and 2% penicillin/streptomycin. Samples with the lowest Ct values from two male patients (63 and 57 years old) suffered by severe pneumonia were selected for isolation attempts. Following filtration through 0.22μm sterile membrane filters (Merck Millipore, Darmstadt, Germany), nasopharyngeal swabs were inoculated onto African green monkey kidney (Vero E6, ATCC: CRL-1586) cells, obtained from the cell culture collection of the Department of Virology, Ankara University Faculty of Veterinary Medicine. The cells were incubated in 5% CO_2 at 37 °C in DMEM, supplemented with 5% fetal bovine serum, L-glutamine, 100U/mL penicillin and 100ug/mL streptomycin. They were monitored daily for cytopathic effects. Detection of the isolated virus was performed by RT-PCR and viruses isolated in the study were named as SARS-CoV-2-Ank1 and SARS-CoV-2-Ank2. We performed three consecutive plaque assays (PA) for purifying the isolates. In each PA, Vero E6 cells grown in 6-well plates were infected with 10-fold dilutions of the isolates. After one-hour incubation at 37 °C, the cells were overlaid by molten media (1:1 ratio of SeaPlaque Low Melting agarose, Lonza, USA and 2xDMEM) and incubated for three days. Plaques were visualized by adding neutral red at 72 h post-inoculation (hpi). Three individually well-separated plaques were collected and used for the next plaque purification step.

The stock viruses were produced from the purified viruses in Vero E6 cells in T75 culture vessels. Infected cells were frozen when cytopathic effect (CPE) reached 80% of the monolayer and subsequently thawed and cleared by centrifugation at 3000 rpm for 15 min at 4 °C. The culture supernatant was then aliquoted in 500 μL and stored at -80 °C for further bioassays. The virus was inactivated at 60 °C for 90 min for imaging.

2.3. In vitro infectivity and one-step growth curve

Virus infectivity was detected with the Tissue Culture Infective Dose 50% ($TCID_{50}$) protocol. Briefly, 100 μL of 10-fold dilutions of each virus were inoculated in quadruplicate on Vero E6 cells grown in 96-well microtiter plates. Infected cells were incubated at 37 °C until virus controls showed 100% CPE. The $TCID_{50}$ was determined according to Reed and the Muench method (Reed and Muench, 1938). In vitro growth characteristic of both isolates was analyzed by means of one-step growth curves. For this purpose, we infected series of Vero E6 cells grown in T25 culture flasks at a 0.01 MOI of the viruses. After one-hour incubation at 37 °C, cells were fed with 5 mL serum free DMEM and one flask was frozen immediately as 0 time point which was followed by freezing the remaining flasks every six hours. Each time point was then titrated as described above.

2.4. Genomic RNA isolation and quantitative RT-PCR

Genomic RNA was extracted using TRIzol reagent (Thermo Fisher Scientific, USA) according to manufacturer instructions. The final RNA pellet was resuspended in 100 μL sterile water and used for RT-PCR. The amplification was performed using probe-based Quantinova Pathogen reaction mix (Qiagen, USA) with primers (SF1 and SR1) and probe (SPr) (Supplement1). Reaction conditions were adjusted as described by the manufacturer.

A 774-bp long fragment of the S gene of SARS-CoV-2-Ank1 isolate was amplified using the primers SF2 and SR2 (Supplement 1) in a 30 μL reaction volume using QIAGEN One-step RT-PCR mix (Qiagen, USA). The PCR product was analyzed on a 1% agarose in Tris-borate-EDTA buffer gel containing Visafe Red gel stain (Vivantis, Malaysia). Purified PCR products were ligated into a TA cloning vector pMD19-T (Takara, Japan) and transformed into DH5a *Escherichia coli* competent cells. Confirmation of clones containing recombinant plasmid was achieved by PCR. DNA plasmid concentrations (C) were measured as the absorbance at 260 nm (NanoDrop, Wilmington, DE, USA) and copy number (N) of the plasmid was calculated using the following equation: $N=(C \times 6.02 \times 10^{23})/$ plasmid MW (molecular weight).

2.5. Genome sequencing and data analysis

For initial whole genome sequencing, we used the commercial amplicon-based next generation sequencing panel, CleanPlex® SARS-CoV-2 (Paragon Genomics, Hayward, California, United States), as directed by the manufacturer, in a NextSeq 500 instrument (Illumina, San Diego, California, United States). We further performed Sanger sequencing for confirmation of the virus structural regions. For this

purpose, S, ORF3a, E, M, ORF6, Orf7a, ORF8, N and ORF10 regions of the viral genome were amplified using a set of 21 forward and reverse primers, covering nucleotides 21393–29791 on the SARS-CoV-2 isolate Wuhan-Hu-1 (GenBank accession: NC045512.2) (Supplement 1). The amplicons were then bi-directionally sequenced using BigDye Terminator v3.1 Cycle Sequencing Kit (Thermo Fisher Scientific, Hennigsdorf, Germany) in an ABI PRISM 3500xL Genetic Analyzer (Thermo Fisher Scientific, Hennigsdorf, Germany).

Obtained sequences were handled using Geneious version 11.1.5 (Biomatters Ltd, Auckland, New Zealand). Alignment and pairwise sequence comparisons were generated using CLUSTAL W (Thompson et al., 1994). Recombination screening was undertaken using default algorithms in the RDP4 software (Martin et al., 2015). Alignment and pairwise comparison of nucleotide sequences were generated using CLUSTAL W (Thompson et al., 1994). Evolutionary history was inferred via the maximum-likelihood method using MEGAX, based on the optimal substitution model, estimated individually for each alignment according to the Bayesian information criteria (Kumar et al., 2018).

2.6. Atomic force microscopy (AFM) and scanning electron microscopy (SEM)

Imaging and size distribution analysis of inactivated SARS-CoV-2 isolate Ank1 were performed using AFM and SEM. Heat inactivated virus was analyzed in an Asylum Research MFP-3D AFM (Oxford Instruments, USA) at the image analysis laboratory of UNAM, Bilkent University. Inactivated solutions (20 µl) were dropped on mica surfaces for overnight drying. Samples were characterized in tapping mode using Si probes with a nominal spring constant of 40 N m−1 and a resonance frequency of 300 kHz (Ted Pella Inc., USA). Additionally, inactivated viral samples were imaged with environmental scanning electron microscopy (Technia; FEI, USA). A total of 20 µl of inactivated viral samples were placed on a piece of silicon wafer. Samples were coated with 5 nm of gold/palladium using a sputter coater and investigated using SEM. The size distribution of the inactivated viral particles was analyzed using Zetasizer Nano ZSP.

2.7. Infectivity in IFNAR −/− mice

The IFNAR−/− mice were inoculated (in duplicate) intranasally with 100 µL (50 µL to each nostril) of 1000$TCID_{50}$ SARS-CoV-2 isolate Ank1 under intraperitoneal ketamine (200 mg/kg) and xylazine (10 mg/kg) anesthesia. The mice were observed twice a day for symptoms including appearance changes (erected hairs), depression, weight loss, and death during the next 13 days' post challenge. Blood samples were collected from the tail vein on days 7 and 14 (time of sacrifice) and were used in virus neutralization assay. Tissue samples (e.g. lungs, jejunum, liver, heart and kidneys) were taken and used for virus quantification and immunohistochemistry (IHC) and histopathologic examinations. Besides, lung homogenate was used next animal inoculation. Virus loads in tissues were determined using the real-time RT-PCR in the tissues. Two wild-type mice were also infected as described above with the identical virus as controls.

2.8. Virus neutralization assay (VNA)

Presence of virus specific neutralizing antibodies in the infected IFNAR−/− mice were evaluated via VNA. Briefly, the serum samples were inactivated at 56 °C for 30 min in a water bath. The serially-diluted (two-fold in DMEM) serum samples were mixed with an equal volume of 100$TCID_{50}$ virus (1:10000) titer in duplicate, and incubated for 1 h at 37 °C. The serum–virus mixtures were subsequently inoculated onto one-day-old 90% confluent Vero E6 cells and were grown in 96-well plates. The infected cells were further incubated under the identical conditions for four days. The test was evaluated via inverted microscope when 100% CPE was observed in virus control wells.

2.9. Histopathology and IHC

Animals were sacrificed and necropsied in ABSL-3 conditions. Tissues were fixed in buffered formalin (10%) solution, and standard 4uM tissue sections were prepared following paraffin embedding. Sections were stained with Hematoxylin and Eosin (HE) and examined under light microscope. Tissue sections were also stained immunohistochemically after antigen retrieval with citrate buffer and quenching for intrinsic peroxidase with 3% H_2O_2. Purified SARS-CoV-2 IgG from convalescent human plasma was used as primary antibody, which was followed by incubation with HRPO labelled anti-human IgG secondary antibody (Sigma Aldrich, USA) for an hour. Tissue sections finally were consecutively stained with 3,30 diaminobenzidine tetrahydrochloride (DAB-ThermoScientific, USA) and HE as a counter stain, and visualized microscope (Ziess, Germany) after dehydration and mounting on a slide.

2.10. Statistical analysis

Replication performance of the SARS-CoV-2 isolates was evaluated based on hpi using multiple t-tests (Holm-Sidak method) by GraphPad Prism version 8.0 (GraphPad Software, San Diego, CA, USA; www.graphpad.com). All graphs were created by the same program. Data were considered statistically significant when $p < 0.01$.

3. Results

3.1. Growth characteristics of the isolates

Initial signs of virus growth were observed at 72 hpi, characterized by focally-increased refractility and edging of the cells, followed by rounding and clumping. Microscopy also revealed formation of intensive hyperchromatic cells before detachment (Figure 1). The CPE quickly spread to the entire culture and cytopathology reached 90% of the cells infected on 5 days post-infection (dpi). Subsequent passages performed during plaque purifications resulted in massive destruction of the cells on 5 dpi. Infectivity titers were recorded as $10^{6,25}$ $TCID_{50}$/0.1 mL and 10^{6} $TCID_{50}$/0.1 mL for SARS-CoV-2 isolate Ank1 and SARS-CoV-2 isolate Ank2, respectively. The virus growth curve demonstrated similar time course and infectious progeny yields (Figure 2). However, statistical significance was observed between infectivity titers detected on 12, 18 and 24 hpi using the Holm-Sidak method (p values 0.001098, 0.001244 and 0.000337, alpha = 0.05, each row analyzed individually, without assuming a consistent standard deviation).

3.2. Genome sequencing and diversity

The genomes of the SARS-CoV-2 isolates A1 and A2 comprise 29.868 nucleotides and overall follow the functional topology of the prototype virus Wuhan-Hu-1 (Table 1). On the nucleotide level, the genomes were highly similar, with nucleotide identities of 99.9%, displaying variations in 7 positions (T17432C, T18870C, T25556G, T26728C, G28874A, G28875A, G28876C). Only two amino acid substitutions, occurring in ORF3a (Q57H) and nucleocapsid (N) protein (RG203KR) were noted. The sequences were 99.9% identical to the Wuhan-Hu-1 virus. The neighbor-joining analysis of the complete genome sequences revealed the isolates to be grouped with lineage B1 viruses (Figure 3).

To compare virus genomes and detect probable diversity, we obtained and analysed SARS-CoV-2 sequences submitted from Turkey, publicly available in GenBank (https://www.ncbi.nlm.nih.gov/genbank/) or the GISAID Initiative database (https://www.gisaid.org/). A total of 64 genomes with complete protein coding regions was included in the analyses (Supplement 2). Pairwise comparisons revealed diversities up to 0.6% and 0.2% for nucleotide and deduced amino acids, respectively (region-specific diversities are provided in Table 1). No reliable evidence for recombination was detected among the sequences.

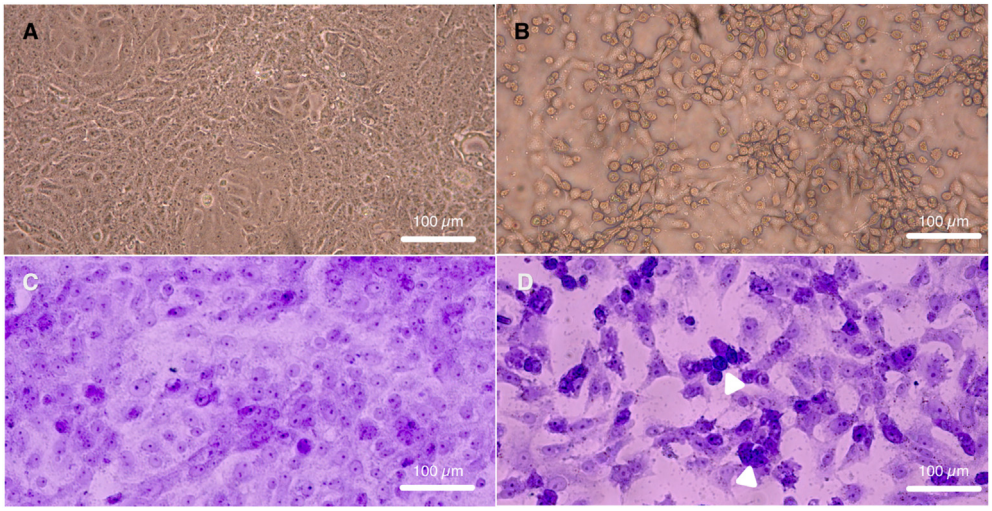

Figure 1. Cytopathology of SARS-Cov-2 Ank-1 isolate in Vero E6 cells. Upper row: (unstained): mock-infected cells (A), virus-infected cells (B); Lower row (crystal violet): mock-infected cells (C), D: virus-infected cells (D). White arrowheads indicate hyperchromatic cells around detached areas.

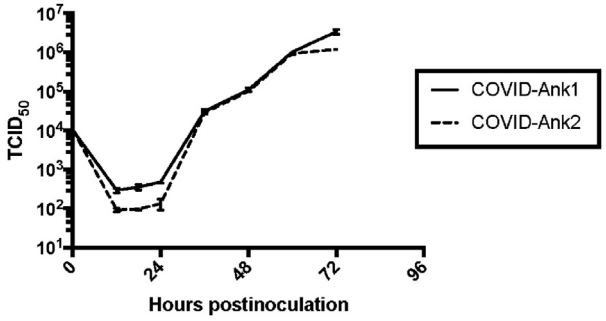

Figure 2. One-step growth curve for SARS-CoV-2-Ank1 and SARS-CoV-2-Ank2 isolates.

We further screened for particular marker variations, frequently used to differentiate SARS-CoV-2 clades (Koyama et al., 2020; Mercatelli and Giorgi, 2020). For markers located in ORF3a (G251V) and ORF8 (L84S), all genomes were observed as identical and belonged in G and L clades. However, the spike protein marker (D614G) varied significantly among viruses, where 28 (43.8%) of the genomes revealed the original aspartic acid residue, which was replaced by glycine in 36 (56.2%) (Table 2). The mutation (A23403G) resulting in this substitution is significant, as it is not only the most frequently-detected mutation worldwide, but likely to impact one of the B cell epitopes located on the S protein of SARS-CoV-2 as well (Koyama et al., 2020; Mercatelli and Giorgi, 2020).

Screening for other previously-described substitutions predicted to affect B and T cell epitopes in S, nucleocapsid (N) and membrane (M) proteins revealed no variations in any of the genomes (Koyama et al., 2020). Of the 20 most common mutations observed worldwide, the genomes revealed changes in 9 positions, with varying frequencies (Table 2). In the S protein, the regions encompassing the ACE2 receptor-binding domain located in the S1 subunit (positions 451–510) were conserved, except for the I468V substitution detected in 3 (4.7%) genomes. Likewise, the polybasic cleavage site (RRAR) and neighboring amino acids (positions 667–694) were retained, except for the single N679K substitution. The two monopartite and one bi-partite nuclear localization signals, associated with fatality and host switch, were identical to the identical to the Wuhan-Hu-1 virus (Gussow et al., 2020).

3.3. Virus imaging

The viral particles were visualized using AFM and SEM. In SEM, the compact, undisturbed viral structures were visualized (Figure 4, panel A, upper row). The viral particles appear mostly intact, albeit with the

Table 1. Functional topology and diversity rates of the SARS-CoV-2 isolates.

Region	Position	Size	Protein	Diversity*
5′UTR	1–258	259	-	-
ORF1a	259–13476	13218	4405	0.7
ORF 1b	13461–21548	8088	2695	0.5
S	21556–25377	3822	1273	0.3
ORF3a	25386–26213	828	275	0.4
E	26238–26465	228	75	0
M	26516–27184	669	222	0.1
ORF6	27195–27380	186	61	0
ORF7a	27387–27752	366	121	0
ORF7b	27749–27880	132	43	0
ORF8	27887–28252	366	121	0.9
N	28267–29526	1260	419	0.5
ORF10	29551–29667	117	38	0
3′UTR	29668–29868	201		

* Indicates maximum deduced amino acid diversity in percent, following removal of ambiguities in alignments.

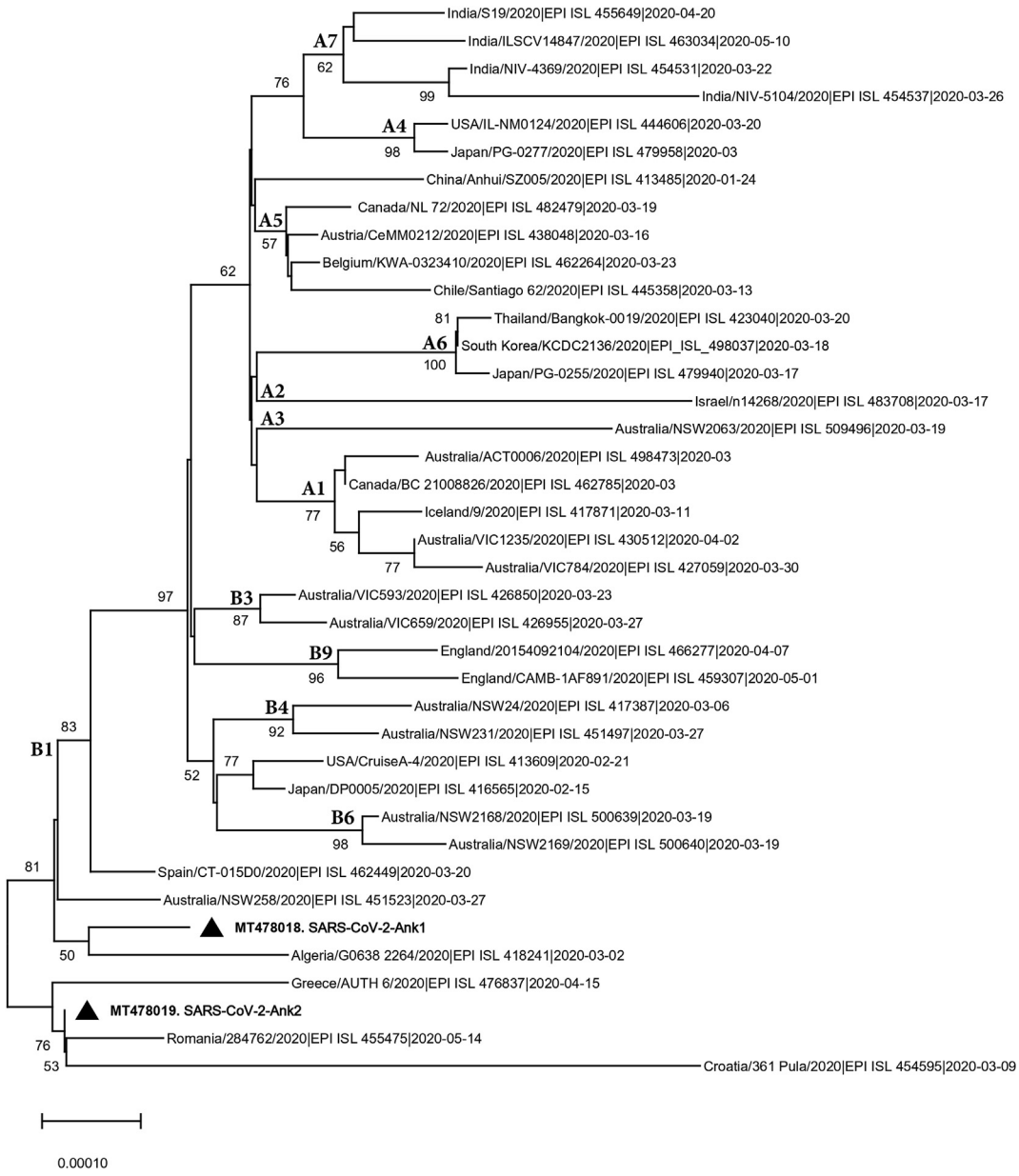

Figure 3. Phylogenetic analysis of the SARS-CoV-2 isolates. The evolutionary history was inferred using the Neighbor-Joining method (Saitou and Nei, 1987). The percentage of replicate trees in which the associated taxa clustered together in the bootstrap test (500 replicates) are shown next to the branches (Felsenstein, 1985). The tree is drawn to scale, with branch lengths in the same units as those of the evolutionary distances used to infer the phylogenetic tree. The evolutionary distances were computed using the Maximum Composite Likelihood method (Tamura et al., 2004) and are in the units of the number of base substitutions per site. This analysis involved 39 nucleotide sequences. All ambiguous positions were removed for each sequence pair (pairwise deletion option). There were a total of 29903 positions in the final dataset. Evolutionary analyses were conducted in MEGA X (Kumar et al., 2018; Stecher et al., 2020). Viruses are indicated by country of detection, isolate name, GISAID database accessiun number and date. Bootstrap values lower than 50 are not shown. Solid triangles indicate local SARS-CoV-2 isolates, Ank1 and Ank2. Main virus lineages are shown on the tree (Rambaut et al., 2020).

destruction of few virions, showing damaged capsid structure with potential nucleic acid loss. AFM imaging showed the morphology of the viral particles (Figure 4, panel A, lower row). Additionally, we checked the size distribution of inactivated SARS-CoV-2 viruses. which was observed as broad (Figure 4, panel B). This suggests that either viral particles clumped at different sizes, or the inactivation triggered a reversible disassembly of the viral capsids. Once the inactivation temperature is removed, the particles may maintain under non-stress conditions. The overall size distribution in AFM was consistent with SEM imaging.

3.4. Virus infection in mice

The SARS-CoV-2 isolates produced non-fatal infection in IFNAR−/− mice during 14 days. Daily inspections revealed humped back and erected hairs, while body temperature and weight remained within normal limits. Animals were bled from tail vein on days 7 and 14 to check seroconversion via VNT. Serum samples withdrawn on 14 dpi showed neutralizing antibody with varied median neutralizing antibody titers (Table 3). On necropsy, we detected gross findings in lungs with hyperemia, regional consolidation and subpleural air accumulation (Figure 5).

Table 2. Occurence of the 20 most frequent mutation events observed in SARS-CoV-2 genomes.

Mutation	Target	Outcome	Frequency (%)
C1059T	NSP2	amino acid change (T85I)	3.1
G1440A	NSP2	amino acid change (G212D)	0
ATG1605del	NSP2	deletion	0
A2480G	NSP2	amino acid change (I559V)	0
C2558T	NSP2	amino acid change (P585S)	0
C3037T	NSP3	silent	64.1
C8782T	NSP4	silent	3.1
G11083T	NSP6	amino acid change (L37F)	35.9
C14408T	NSP12b	amino acid change (P314L)	62.5
C14805T	NSP12b	silent	0
T17247C	NSP13	silent	0
C17747T	NSP13	amino acid change (P504L)	0
A17858G	NSP13	amino acid change (Y541C)	0
C18060T	NSP14	silent	0
A23403G	S	amino acid change (D614G)	56.2
G25563T	ORF3a	amino acid change (Q57H)	40.6
G26144T	ORF3a	amino acid change (G251V)	0
T28144C	ORF8	amino acid change (L84S)	1.6
GGG28881AAC	N	amino acid change (RG203KR)	15.6

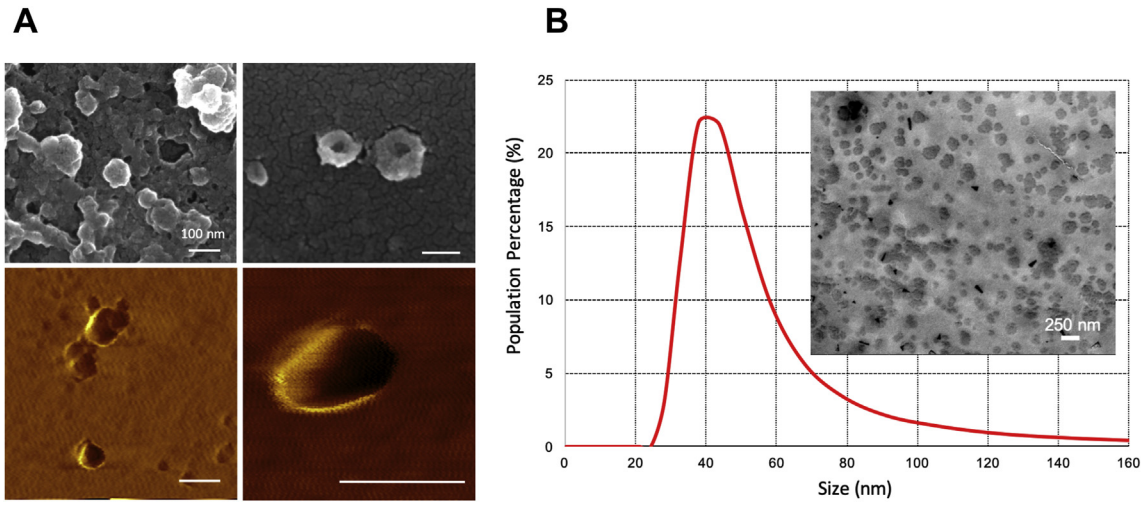

Figure 4. Imaging of the SARS-Cov-2 Ank-1 isolate using environmental SEM (Panel A – upper row) and AFM (Panel A – lower row). Size distribution of the viral particles (Panel B).

Table 3. Viral loads and neutralizing antibodies in experimentally-infected mice.

Passage	Animal	Virus Load (RNA copy/mL)						Serology*	
		Lung	Jejunum	Spleen	Liver	Kidney	Heart	7dpi	14dpi
1	1	14890	<100	<100	2606	9903	<100	-	1/16
	2	9750	<100	<100	<100	5388	-	-	1/16
2	1	2560	-	<100	157	978	<100	-	1/8
	2	7700	<100	140	<100	2839	-	-	1/16

* Given as reciprocals of serum dilutions 50% neutralizing (SN_{50}) 100$TCID_{50}$ of SARS CoV-2; (-) negative.

Virus loads in tissues were determined by quantitative real-time RT-PCR. Limit of detection (LOD) of the system was observed as 100 copy/μL. Measurable virus RNA was detected in lung, liver and jejunum samples of the infected animals (Table 3). No evidence for infection by RT-PCR or histopathology was observed in controls.

3.5. Histopathology and IHC in mice

Tissues including lungs, heart, stomach, intestines, liver, spleen and kidneys from both mice revealed similar histopathological and immunohistochemical findings. Microscopically, no significant

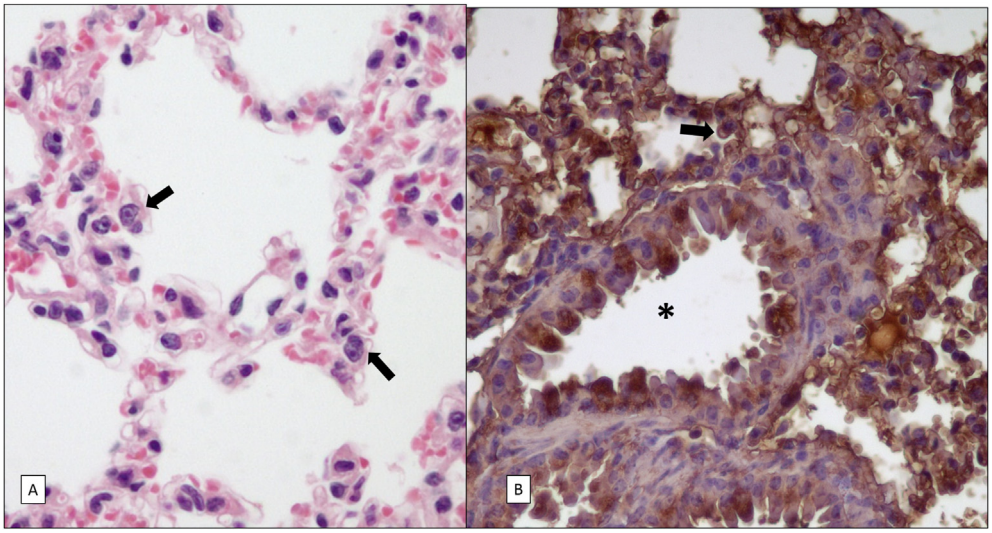

Figure 5. Hematoxlyin-eosin (A) and IHC (B) staining of respiratory epithelium in the IFNAR−/− mouse with prominent lung findings. Alveoli are lined by some pneumocytes with marked cellular atypia such as nuclear enlargement and prominent nucleoli (arrows) (A). In IHC, pneumocytes (arrow) and respiratory epithelium lining this bronchiole (asterix) showed strong cytoplasmic and staining (B).

histomorphologic change was observed in most tissues, except that some pneumocytes showed cytologic atypia characterized by nuclear enlargement, irregular nuclear contours, and prominent nucleoli in one individual (Figure 6). Immunohistochemically, we observed large areas of strong cytoplasmic and membranous staining in the following tissues: respiratory epithelium and pneumocytes of the lungs, enterocytes of intestinal villi and crypts, hepatocytes and biliary ductal epithelium, particularly the histocytes of the spleen, and renal tubular epithelial cells. Occasionally, weak-to-moderate signals were also seen in cardiac myocytes and gastric glands (Figure 6).

4. Discussion

In this study, we describe the isolation and genome sequencing of two SARS-CoV-2 isolates from infected humans in Turkey, viral replication kinetics in Vero E6 cells and outcome of infection in experimentally-infected IFNAR−/− mice. The lack of innate antiviral interferon signaling makes Vero E6 one of the frequently-used cell lines for virus isolation (Emeny and Morgan, 1979). We accomplished isolation without TPCK-treated trypsin to facilitate virus attachment. Similar to SARS-CoV (Kaye, 2006), we observed Vero E6 lines to support SARS-CoV-2 replication and produce high titers of virus with prominent CPE. The epithelium is often the first site of replication in respiratory viruses, including coronaviruses (Matrosovich et al., 2004; Zhang et al., 2002). SARS-CoV-2 needs to bind angiotensin-converting enzyme 2 (ACE2) receptor expressed on the host cell membrane. Vro E6 cells express ACE2 receptor on their apical plasma membrane (Ren et al., 2006). In our study, isolation and further cultivation trials were successfully performed in Vero E6 cells to high titers ($>10^7$/mL) with rapidly-developing cytopathic effect in each passage. Regarding replication performance, we noticed slight differences between two isolates in terms of virus yields harvest during early replication. However, this was not further explored during subsequent passages.

Whole genome sequencing of the isolates revealed that the viruses were well-conserved, with less than 1% diversity compared to the prototype SARS-CoV-2 Wuhan-Hu-1. Following the pandemic spread, the low variability of SARS-CoV-2 genomes has been widely observed, owing to the available rapid sequencing technologies and data sharing platforms. Currently, over 50,000 viral genomic sequences have been made publicly-available, enabling near real-time evaluation of genomic variations during spread (Shu and McCauley, 2017). A large-scale analysis calculated an average of 6.7 mutations per genome, as compared to the reference virus (Mercatelli and Giorgi, 2020). The grouping of global viruses into three main clades, namely, G, S and V, according to specific marker mutations in the genome has been widely used. Moreover, a recently-proposed system clusters global SARS-CoV-2 isolates into main lineages A and B, with sublineage designations indicated with numbers (Rambaut et al., 2020). According to this classification, SARS-CoV-2 isolates Ank1 and Ank2 are grouped within the lineage B1, mostly representing viruses from European outbreaks with further global expansion. Our analyses of the viral genomes obtained in this study, as well as the available complete genomes from Anatolia further showed very limited diversity (up to 0.2% on deduced amino acids), no variation in markers located in ORF3a and ORF8, and no evidence of recombination. The most prominent variation is observed on the spike protein marker, resulting in the substitution D614G, with a prevalence of 56.2%. This substitution may be associated with significant consequences for virulence and immune response. It is highly-prevalent in Europe, particularly in Netherlands, Switzerland and France, as well as in Brazil (Koyama et al., 2020). Experimental evidence suggests that viruses possessing the substitution has limited shedding of the spike S1 domain, increased S-protein incorporation into the virion, resulting in enhanced transmission (Zhang et al., 2020). Moreover, it is likely to cause a change in the virus B-cell antigenic epitopes, due to the alterations in size and hydrophobicity profile, with unknown consequences on immunogenicity and antibody-dependent virus neutralization (Koyama et al., 2020). Therefore, it must be considered in prospective vaccine studies, prolonged immune response and cross-protection evaluations. We have not performed a comprehensive phylogenetic evaluation in this study. Nevertheless, a recent analysis, albeit with a lower number of genomes, suggested multiple independent international virus introductions in Anatolia and inland spread (Adebalı et al., 2020).

Finally, we inoculated IFNAR−/− mice with the local SARS-CoV-2 isolates, for a preliminary evaluation of infection dynamics in a small animal model. SARS-CoV-2 infects mice inefficiently, due to the variations in ACE2 structure, serving as the virus receptor. Hence, transgenic expression of human ACE2 for enhanced susceptibility to the virus has been attained in various mice breeds and such models have been widely-used for COVID-19 research (Bao et al., 2020; Jiang et al., 2020). Mice transgenic for hACE2 have been developed as an animal model for SARS-CoV-2 infection, and it presents as a non-lethal disease with an RNA load of $10^{6.77}$ copies/ml or $10^{2.44}$ $TCID_{50}$/100 µl at 3 dpi (Bao et al., 2020). In addition, Syrian hamsters were also found susceptible to SARS-CoV-2 infection with mild disease starting at 2 dpi and viral load as

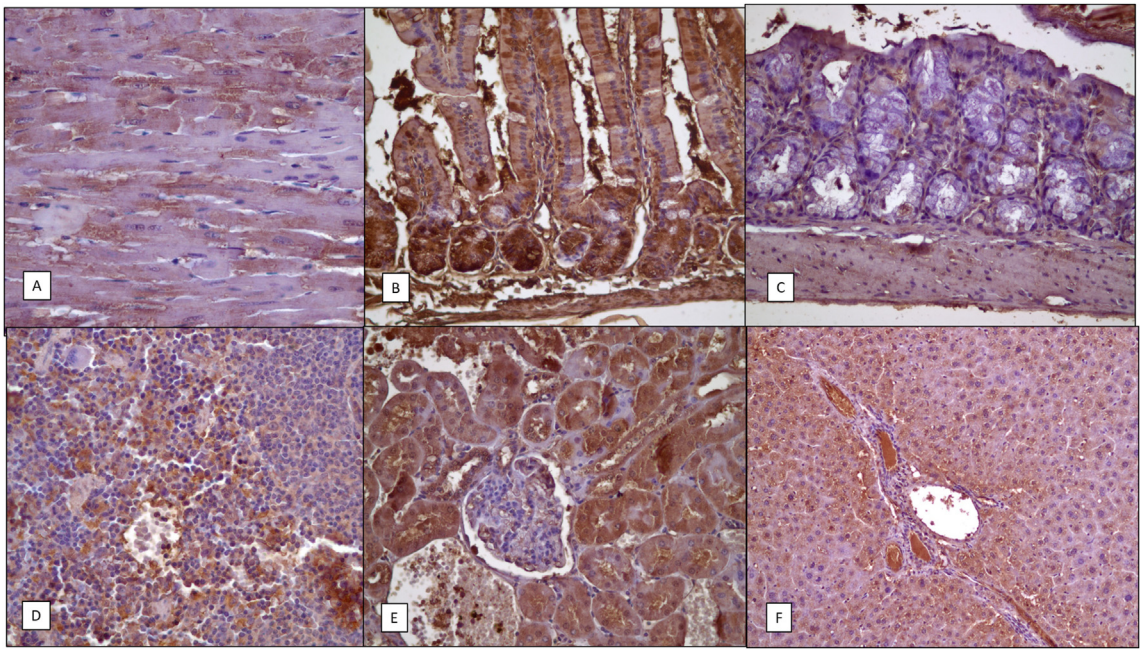

Figure 6. IHC staining in other tissues. Patchy immunoreactivity is seen in cardiac myocytes (A). In the gastrointestinal tissue, staining is strong and diffuse in the epithelium of small intestines (B), whereas only scattered glandular cells are positive in the stomach (C). In the spleen, interfollicular histiocytes are positive (D). In this image from the kidney shows a glomerulus at the center, which is negative, and tubular epithelium with diffuse and strong staining (E). A patchy staining is also noted in hepatocytes as well as ductal epithelial cells in the liver (F).

high as 10^5-10^7 $TCID_{50}$/g in the lung. The animals recovered from the infection about 7 dpi (Chan et al., 2020). Wild-type C57BL/6 and recombinant virus inoculated BALB/c mice were investigated as other potential small animal models as well (Dinnon et al., 2020; Sun et al., 2020). In the IFNAR−/− mice, local SARS-CoV-2 isolates were non-fatal within two weeks of inoculation and only mild symptoms were noted, with neutralizing antibodies being detectable on the 14 day post-inoculation. Quantitative RNA measurements and IHC showed probable viral replication in several internal organs including lungs, liver, spleen, kidneys, heart and the gastrointestinal system. These findings suggest that the virus causes a systemic infection in IFNAR−/− mice. The gross findings and relative viral loads further indicate lungs as the main site of viral replication, with cellular atypia observed in tissue sections (Figure 5). These observations require further confirmation in larger cohorts. In this study, we observed a decreased amount of virus load in tissues after both passages. This could be due to the low recovery of viruses from tissues since the animals sacrificed on 14 dpi. Also, the presence of diffuse infection in the proximal tubule epithelium of the kidney suggests the possibility of the virus shedding via urine, which was documented in human infections as well (Guan et al., 2020). The IFNAR−/− mice require attention as alternate models for SARS-CoV-2 studies.

In conclusion, we characterized two local SARS-CoV-2 isolates, studied in vitro growth dynamics in Vero E6 cells and presented transgenic type I interferon knockout mice as usable animal model for vaccine or drug trials.

Declarations

Author contribution statement

Alireza Hanifehnezhad: Conceived and designed the experiments; Analyzed and interpreted the data; Wrote the paper.

Ebru Şahin Kehribar, Sevgen Önder, Engin Yılmaz: Performed the experiments; Analyzed and interpreted the data.

Sıdıka Öztop, Ali Sheraz, Serkan Kasırga: Performed the experiments.

Koray Ergünay: Performed the experiments; Analyzed and interpreted the data; Wrote the paper.

Erkan Yılmaz, Doruk Engin, T. Çiğdem Oğuzoğlu: Contributed reagents, materials, analysis tools or data.

Urartu Özgür Şafak Şeker: Performed the experiments; Analyzed and interpreted the data; Contributed reagents, materials, analysis tools or data; Wrote the paper.

Aykut Özkul: Conceived and designed the experiments; Performed the experiments; Analyzed and interpreted the data; Contributed reagents, materials, analysis tools or data; Wrote the paper.

Funding statement

This work was supported by the Scientific and Technological Research Council of Turkey (TÜBİTAK, Grant No: T1004 -18AG020), under the framework “COVID-19 Turkey Platform”.

Competing interest statement

The authors declare no conflict of interest.

Additional information

Supplementary content related to this article has been published online at https://doi.org/10.1016/j.heliyon.2020.e05116.

References

Adebalı, O., Bircan, A., Çırcı, D., İşlek, B., Kilinç, Z., Selçuk, B., Turhan, B., 2020. Phylogenetic analysis of SARS-CoV-2 genomes in Turkey. Turk. J. Biol. 44, 146–156.

Andersen, K.G., Rambaut, A., Lipkin, W.I., Holmes, E.C., Garry, R.F., 2020. The proximal origin of SARS-CoV-2. Nat. Med. 26, 450–452.

Bao, L., Deng, W., Huang, B., Gao, H., Liu, J., Ren, L., Wei, Q., Yu, P., Xu, Y., Qi, F., Qu, Y., Li, F., Lv, Q., Wang, W., Xue, J., Gong, S., Liu, M., Wang, G., Wang, S., Song, Z., Zhao, L., Liu, P., Zhao, L., Ye, F., Wang, H., Zhou, W., Zhu, N., Zhen, W., Yu, H., Zhang, X., Guo, L., Chen, L., Wang, C., Wang, Y., Wang, X., Xiao, Y., Sun, Q., Liu, H., Zhu, F., Ma, C., Yan, L., Yang, M., Han, J., Xu, W., Tan, W., Peng, X., Jin, Q., Wu, G., Qin, C., 2020. The pathogenicity of SARS-CoV-2 in hACE2 transgenic mice. Nature.

Chan, J.F., Zhang, A.J., Yuan, S., Poon, V.K., Chan, C.C., Lee, A.C., Chan, W.M., Fan, Z., Tsoi, H.W., Wen, L., Liang, R., Cao, J., Chen, Y., Tang, K., Luo, C., Cai, J.P., Kok, K.H., Chu, H., Chan, K.H., Sridhar, S., Chen, Z., Chen, H., To, K.K., Yuen, K.Y., 2020. Simulation of the clinical and pathological manifestations of Coronavirus Disease 2019 (COVID-19) in golden Syrian hamster model: implications for disease pathogenesis and transmissibility. Clin. Infect. Dis ciaa325.

Chen, Y., Liu, Q., Guo, D., 2020. Emerging coronaviruses: genome structure, replication, and pathogenesis. J. Med. Virol. 92, 418–423.

Coronaviridae Study Group of the International Committee on Taxonomy of V, 2020. The species Severe acute respiratory syndrome-related coronavirus: classifying 2019-nCoV and naming it SARS-CoV-2. Nat. Microbiol. 5, 536–544.

Cui, J., Li, F., Shi, Z.L., 2019. Origin and evolution of pathogenic coronaviruses. Nat. Rev. Microbiol. 17, 181–192.

Dinnon, K.H., Leist, S.R., Schäfer, A., Edwards, C.E., Martinez, D.R., Montgomery, S.A., West, A., Yount, B.L., Hou, Y.J., Adams, L.E., Gully, K.L., Brown, A.J., Huang, E., Bryant, M.D., Choong, I.C., Glenn, J.S., Gralinski, L.E., Sheahan, T.P., Baric, R.S., 2020. A mouse-adapted SARS-CoV-2 model for the evaluation of COVID-19 medical countermeasures. bioRxiv.

Emeny, J.M., Morgan, M.J., 1979. Regulation of the interferon system: evidence that Vero cells have a genetic defect in interferon production. J. Gen. Virol. 43, 247–252.

Felsenstein, J., 1985. Confidence limits on phylogenies: an approach using the bootstrap. Evolution 39, 783–791.

Guan, W.J., Ni, Z.Y., Hu, Y., Liang, W.H., Ou, C.Q., He, J.X., Liu, L., Shan, H., Lei, C.L., Hui, D.S.C., Du, B., Li, L.J., Zeng, G., Yuen, K.Y., Chen, R.C., Tang, C.L., Wang, T., Chen, P.Y., Xiang, J., Li, S.Y., Wang, J.L., Liang, Z.J., Peng, Y.X., Wei, L., Liu, Y., Hu, Y.H., Peng, P., Wang, J.M., Liu, J.Y., Chen, Z., Li, G., Zheng, Z.J., Qiu, S.Q., Luo, J., Ye, C.J., Zhu, S.Y., Zhong, N.S., 2020. China medical treatment expert group for Covid-19, 2020. Clinical characteristics of Coronavirus disease 2019 in China. N. Engl. J. Med. 382, 1708–1720.

Gussow, A.B., Auslander, N., Faure, G., Wolf, Y.I., Zhang, F., Koonin, E.V., 2020. Genomic determinants of pathogenicity in SARS-CoV-2 and other human coronaviruses. Proc. Natl. Acad. Sci. 117, 15193–15199.

Jiang, R.D., Liu, M.Q., Chen, Y., Shan, C., Zhou, Y.W., Shen, X.R., Li, Q., Zhang, L., Zhu, Y., Si, H.R., Wang, Q., Min, J., Wang, X., Zhang, W., Li, B., Zhang, H.J., Baric, R.S., Zhou, P., Yang, X.L., Shi, Z.L., 2020. Pathogenesis of SARS-CoV-2 in transgenic mice expressing human angiotensin-converting enzyme 2. Cell 182, 50–58.

Kaye, M., 2006. SARS-associated coronavirus replication in cell lines. Emerg. Infect. Dis. 12, 128–133.

Koyama, T., Weeraratne, D., Snowdon, J.L., Parida, L., 2020. Emergence of drift variants that may affect COVID-19 vaccine development and antibody treatment. Pathogens 9, 324.

Kumar, S., Stecher, G., Li, M., Knyaz, C., Tamura, K., 2018. MEGA X: molecular evolutionary genetics analysis across computing platforms. Mol. Biol. Evol. 35, 1547–1549.

Martin, D.P., Murrell, B., Golden, M., Khoosal, A., Muhire, B., 2015. RDP4: detection and analysis of recombination patterns in virus genomes. Virus. Evol. 1, vev003.

Matrosovich, M.N., Matrosovich, T.Y., Gray, T., Roberts, N.A., Klenk, H.D., 2004. Human and avian influenza viruses target different cell types in cultures of human airway epithelium. Proc. Natl. Acad. Sci. U.S.A. 101 (13), 4620–4624.

Mercatelli, D., Giorgi, F.M., 2020. Geographic and genomic distribution of SARS-CoV-2 mutations. Preprints.

Rambaut, A., Holmes, E.C., O'Toole, Á., Hill, V., McCrone, J.T., Ruis, C., du Plessis, L., Pybus, O.G., 2020. A dynamic nomenclature proposal for SARS-CoV-2 lineages to assist genomic epidemiology. Nat. Microbiol.

Reed, L.J., Muench, H., 1938. A simple method of estimating fifty per cent endpoints. Am. J. Epidemiol. 27, 493–497.

Ren, X., Glende, J., Al-Falah, M., de Vries, V., Schwegmann-Wessels, C., Qu, X., Herrler, G., 2006. Analysis of ACE2 in polarized epithelial cells: surface expression and function as receptor for severe acute respiratory syndrome-associated coronavirus. J. Gen. Virol. 87, 1691–1695.

Saitou, N., Nei, M., 1987. The neighbor-joining method: a new method for reconstructing phylogenetic trees. Mol. Biol. Evol. 4, 406–425.

Shu, Y., McCauley, J., 2017. GISAID: global initiative on sharing all influenza data–from vision to reality. Euro Surveill. 22, 30494.

Stecher, G., Tamura, K., Kumar, S., 2020. Molecular evolutionary genetics analysis (MEGA) for macOS. Mol. Biol. Evol. 37, 1237–1239.

Su, S., Wong, G., Shi, W., Liu, J., Lai, A.C., Zhou, J., Gao, G.F., 2016. Epidemiology, genetic recombination, and pathogenesis of coronaviruses. Trends Microbiol. 24, 490–502.

Sun, S.H., Chen, Q., Gu, H.J., Yang, G., Wang, Y.X., Huang, X.Y., Liu, S.S., Zhang, N.N., Li, X.F., Xiong, R., Guo, Y., Deng, Y.Q., Huang, W.J., Liu, Q., Liu, Q.M., Shen, Y.L., Zhou, Y., Yang, X., Zhao, T.Y., Fan, C.F., Zhou, Y.S., Qin, C.F., Wang, Y.C., 2020. A mouse model of SARS-CoV-2 infection and pathogenesis. Cell Host Microbe 28, 124–133.

Tamura, K., Nei, M., Kumar, S., 2004. Prospects for inferring very large phylogenies by using the neighbor-joining method. Proc. Natl. Acad. Sci. U.S.A. 101, 11030–11035.

Tang, D., Comish, P., Rui Kang, R., 2020. The hallmarks of COVID-19 disease. PLoS Pathog. 16, e1008536.

Thompson, J.D., Higgins, D.G., Gibson, T.J., 1994. CLUSTAL W: improving the sensitivity of progressive multiple sequence alignment through sequence weighting, position-specific gap penalties and weight matrix choice. Nucleic Acids Res. 22, 4673–4680.

World Health Organization, 2020. Coronavirus Disease (COVID-19) Pandemic. https://www.who.int/emergencies/diseases/novel-coronavirus-2019. (Accessed 17 May 2020).

Zhang, L., Peeples, M.E., Boucher, R.C., Collins, P.L., Pickles, R.J., 2002. Respiratory syncytial virus infection of human airway epithelial cells is polarized, specific to ciliated cells, and without obvious cytopathology. J. Virol. 76, 5654–5666.

Zhang, L., Jackson, C.B., Mou, H., Ojha, A., Rangarajan, E.S., Izard, T., Farzan, M., Choe, H., 2020. The D614G mutation in the SARS-CoV-2 spike protein reduces S1 shedding and increases infectivity. bioRxiv [Preprint], 32587973.